ADVANCED FUNCTIONAL MATERIALS
www.afm-journal.de

Living Cells Directly Growing on a DNA/$Mn_3(PO_4)_2$-Immobilized and Vertically Aligned CNT Array as a Free-Standing Hybrid Film for Highly Sensitive In Situ Detection of Released Superoxide Anions

Fang Xin Hu, Yue Jun Kang, Feng Du, Lin Zhu, Yu Hua Xue, Tao Chen, Li Ming Dai, and Chang Ming Li**

It is important to detect reactive oxygen species (ROS) in situ for investigation of various critical biological processes, and this is however very challenging because of the limited sensitivity or/and selectivity of existing methods that are mainly based on sensing ROS released by cells with short lifetimes and low concentrations in a culture medium. Here, a new approach is reported to directly grow living cells on DNA/$Mn_3(PO_4)_2$-immobilized and vertically aligned carbon nanotube (VACNT) array nanostructure as a smart free-standing hybrid film, of which the DNA/$Mn_3(PO_4)_2$ and VACNT provide high electroactivity and excellent electron transport, respectively, while the directly grown cell on the nanostructure offers short diffusion distance to reaction sites, thus constructing a highly sensitive in situ method for detection of cancer-cell-released ROS under drug stimulations. Compared to the measured ROS released by cells in a culture medium, the detection sensitivity with this constructed hybrid film increases by more than six times, which implies that ROS molecules (superoxide anions) secreted from living cells are immediately captured by this smart structure without diffusion process or with extremely short diffusion distance. This design considerably reduces the time from release to detection of the target molecules, minimizing the potential molecular decay due to the short lifetime or high reactivity.

1. Introduction

Superoxide anions ($O_2^{\bullet-}$) are a typical type of reactive oxygen species (ROS), which are potent oxidizing agents and are formed under a variety of physiological and pathophysiological conditions in all living organisms that require metabolism of oxygen. Overproduction of $O_2^{\bullet-}$ can lead to ischemia–reperfusion or hypoxia and cause damage to brain, proteins, cells, and tissues as well as a wide variety of neurodegenerative diseases.[1,2] In situ monitoring of $O_2^{\bullet-}$ concentrations released from living cells is essential to understand various biological roles of $O_2^{\bullet-}$. However, direct sensing of $O_2^{\bullet-}$ in biological samples is extremely challenging. $O_2^{\bullet-}$ is by nature a highly reactive molecule and is therefore extremely unstable and easy to decay, making it very difficult to detect them directly.[3] Thus most existing methods for detection of $O_2^{\bullet-}$ levels have relied mainly on detecting the end products either by chemiluminescence or fluorescence produced when specific compounds react with $O_2^{\bullet-}$,[4] which is very complicated and imprecise. Therefore, it is critical to establish a reliable and reproducible approach to determine $O_2^{\bullet-}$ in situ, facilitating investigations of physiological and pathological processes related to $O_2^{\bullet-}$.

For this purpose, manganese (Mn) compounds have proved to be reliable catalysts for $O_2^{\bullet-}$.[5] A recent work reported a manganous phosphate ($Mn_3(PO_4)_2$) nanosheet-based biosensor to detect $O_2^{\bullet-}$ and investigated the related catalytic mechanism.[6] However, the detection of $O_2^{\bullet-}$ was performed on cell culture in a petri dish subjected to drug stimulation, where the cell-released $O_2^{\bullet-}$ molecules need to diffuse through medium solution to access the surface of sensing electrode. Due to extremely short life time, many $O_2^{\bullet-}$ molecules will decay during the diffusion leading to an underestimation of the $O_2^{\bullet-}$ released by each cell. Alternatively, if the cells are directly cultured on a sensing platform, the released $O_2^{\bullet-}$ can be rapidly captured and detected by the catalysts, which will improve the accuracy of the measurement considerably.

F. X. Hu, Prof. Y. J. Kang, Prof. C. M. Li
Chongqing Key Laboratory for Advanced Materials and Technologies of Clean Energies
Institute for Clean Energy and Advanced Materials
Chongqing 400715, P. R. China
E-mail: ecmli@swu.edu.cn

F. X. Hu, Prof. Y. J. Kang, Prof. C. M. Li
Chongqing Engineering Research Center for Rapid Diagnosis of Dread Disease
Chongqing 400715, China

F. X. Hu, Prof. Y. J. Kang, Prof. C. M. Li
Faculty of Materials and Energy
Southwest University
Chongqing 400715, P. R. China

F. X. Hu, Dr. F. Du, Dr. L. Zhu, Dr. Y. H. Xue, Prof. T. Chen, Prof. L. M. Dai
Center of Advanced Science and Engineering for Carbon (Case4Carbon)
Department of Macromolecular Science and Engineering
Case Western Reserve University
10900 Euclid Avenue
Cleveland, OH 44106, USA
E-mail: liming.dai@case.edu

DOI: 10.1002/adfm.201502341

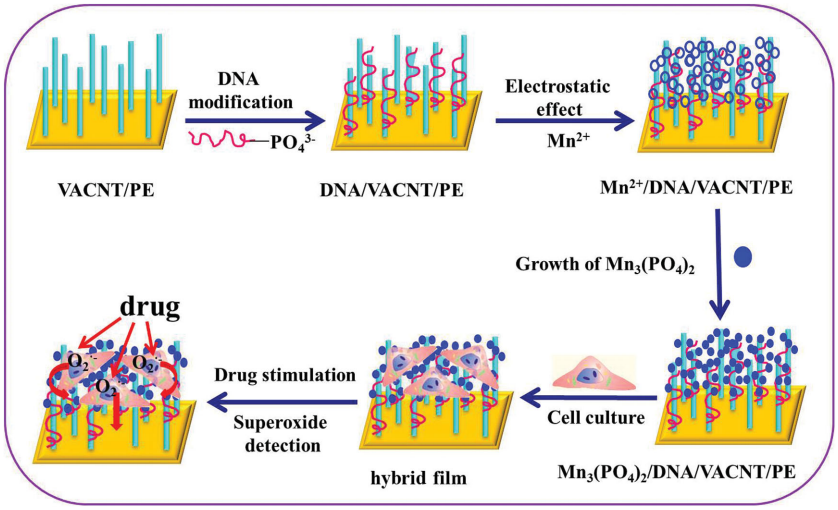

Scheme 1. Schematic illustration of the preparation procedure for the MDA-MB-231/$Mn_3(PO_4)_2$/DNA/VACNT/PE hybrid film and its living cell assay.

Compared with other methods, electrochemical techniques have been widely used for efficient detection of cellular molecules in situ.[7] An ideal biological-electrochemical hybrid film should not only maintain high conductivity with excellent catalytic activity for efficient signal generation and transport but also exhibit good biocompatibility to both cells and surrounding environment.[8,9] In this context, vertically aligned carbon nanotube (VACNT) arrays have been used in fuel cells,[10] supercapacitors,[11] and genetic engineering,[12] showing excellent electrochemical and biological properties. The main advantage of VACNT over the carbon nanotubes (CNT) is its regular arrangement instead of the random stocked CNT, which can not only enhance the conductivity but also could shorten the diffusion distance of the reactant for enhanced sensing performance. Thus, VACNT array can be a desirable platform for an electrochemical detection substrate.

In this study, we report a free standing hybrid film using VACNT array supported by polyethylene (VACNT/PE) as a cell culture and electrocatalytic platform together with $Mn_3(PO_4)_2$ as the biomimetic superoxide dismutase for sensing $O_2^{\bullet-}$ in situ. DNA chains, having a strong affinity to CNT[13] and also abundant PO_4^{3-}, were used as negatively charged molecular linkers for efficient deposition of $Mn_3(PO_4)_2$ onto VACNT/PE film. Living human breast carcinoma cells (MDA-MB-231) were directly cultured on the resultant 3D $Mn_3(PO_4)_2$/DNA/VACNT/PE hybrid film for in situ detection of $O_2^{\bullet-}$, as shown in **Scheme 1**. The proposed MDA-MB-231/$Mn_3(PO_4)_2$/DNA/VACNT/PE hybrid film ensures sensitive and accurate in situ measurement of $O_2^{\bullet-}$ released from the cultured cells under drug stimulation due to excellent electrocatalytic performance and biocompatibility. Compared to the conventional $O_2^{\bullet-}$ detection on living cells cultured in a petri dish, this reported platform delivers much higher sensitivity, faster response and more reliable measurement.

2. Results and Discussion

2.1. Properties of the Hybrid Film

The structure and morphology of different modified films were characterized with scanning electron microscopy (SEM). **Figure 1**A showed the cross-sectional view of VACNT/PE film, which comprised densely packed nanotubes with a length of around 80 μm and aligned perpendicularly to the substrate. The corresponding top-view image of VACNT/PE film was showed in Figure S1A (Supporting Information), indicating the presence of some pores randomly through the VACNT array due to relatively low packing density, which was beneficial for the cell growth. After water plasma treatment, the VACNT/PE film still retained their well-aligned structure as shown in Figure 1B. From the top-view image of water plasma treatment VACNT/PE film (Figure S1B, Supporting Information), more pores could be observed. Compared to plain VACNT/PE film (Figure 1A), DNA/VACNT/PE film became smoother with DNA covering the surface of VACNT array (Figures 1C and S1C, Supporting Information). On the $Mn_3(PO_4)_2$/VACNT/PE film without DNA modification (Figures 1D and S1D, Supporting Information), some accumulation of VACNT arrays on the surface could be observed,

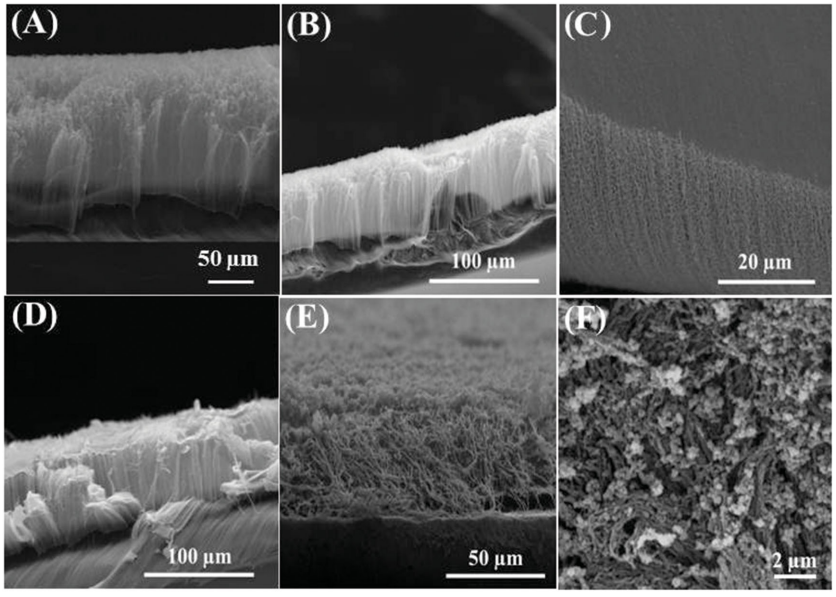

Figure 1. Cross-section SEM image of A) VACNT/PE film, B) water plasma treated VACNT/PE film, C) DNA/VACNT/PE film, D) $Mn_3(PO_4)_2$/VACNT/PE film, E) $Mn_3(PO_4)_2$/DNA/VACNT/PE film, and F) top view SEM image of $Mn_3(PO_4)_2$/DNA/VACNT/PE film.

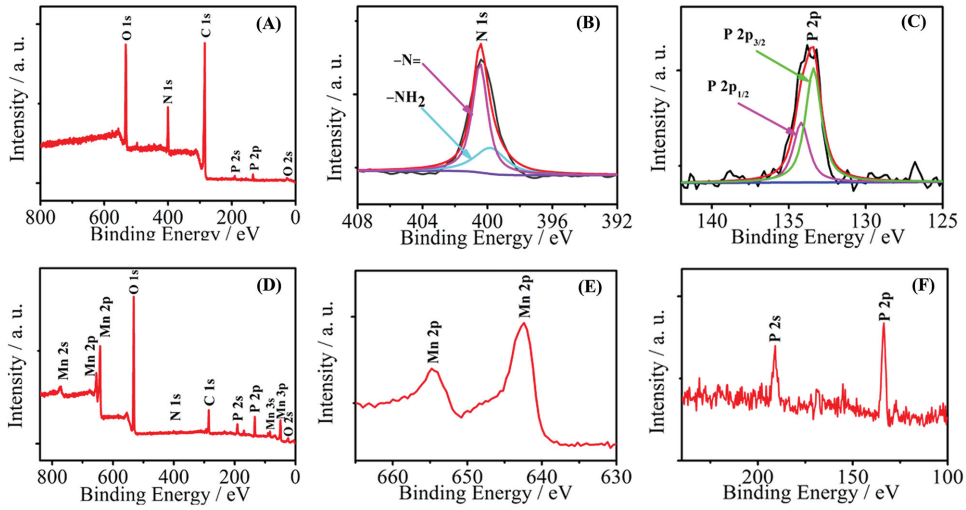

Figure 2. XPS analysis about A) wide scan survey spectra of DNA/VACNT array, B) N 1s spectra in DNA/VACNT array, C) P 2p spectra in DNA/VACNT array, D) wide scan survey spectra of $Mn_3(PO_4)_2$/DNA/VACNT array, E) Mn 2p spectra in $Mn_3(PO_4)_2$/DNA/VACNT array, and F) P 2s and P 2p spectra in $Mn_3(PO_4)_2$/DNA/VACNT array.

although there were few $Mn_3(PO_4)_2$ particles. Figure 1E exhibited the cross-section of $Mn_3(PO_4)_2$/DNA/VACNT/PE film still showing a well-defined array structure, while $Mn_3(PO_4)_2$ nanoparticles mainly distributed on the surface of DNA/VACNT/PE substrate (Figure 1F).

Furthermore, X-ray photoelectron spectroscopy (XPS) measurements were conducted to obtain detailed information about the element composition of different modified VACNT array. **Figure 2**A showed the wide scan survey spectra of DNA/VACNT array, C 1s, O 1s, O 2s, N 1s, P 2s, and P 2p peaks were observed at 284.8, 532.1, 23.6, 400.4, 190.8, and 133.8 eV, respectively. DNA was expected to be strongly immobilized on VACNT array surface due to the presence of N and P elements. For details, N 1s spectra (Figure 2B) contained two peaks centered at 399.8 and 400.5 eV, which could be assigned as conjugated N sp^2 (399.8 eV) and amine group $–NH_2$ or nonconjugated N sp^3 (400.5 eV) belonging to cytosine-base oligomer.[14] Another important feature that strongly confirmed the presence of DNA on VACNT array was the P 2p region as showed in Figure 2C. P 2p could be divided into two peaks around 133.4 and 134.2 eV, associated with P $2p_{3/2}$ and P $2p_{1/2}$, respectively. In the wide scan survey XPS spectra of $Mn_3(PO_4)_2$/DNA/VACNT array (Figure 2D), many elements could be detected such as C 1s (285.2 eV), O 1s (532.0 eV), O 2s (25.6 eV), N 1s (400.8 eV), P 2s (191.2 eV), P 2p (134.0 eV), Mn 2s (771.2 eV), and Mn 2p (654.8 eV, 642.4 eV). The Mn 2p and P 2p spectra were showed in Figure 2E,F, respectively. The surface atomic concentrations of elements were summarized in **Table 1**. The relative concentration ratio between Mn^{2+} and PO_4^{3-} was 1.6, which was almost the same as the atomic ratio in $Mn_3(PO_4)_2$, indicating successful synthesis of $Mn_3(PO_4)_2$ on VACNT array.

Table 1. Elemental surface analysis (by XPS) of different modified VACNT array.

Sample	C [at%]	O [at%]	P [at%]	Mn [at%]	N [at%]
DNA/VACNT	66.7	20.9	1.1	0	11.3
$Mn_3(PO_4)_2$/DNA/VACNT	22.57	52.17	8.99	14.76	1.51

2.2. Effect of Water Plasma Treatment on VACNT/PE Film

As shown in **Figure 3**A, the as-prepared VACNT/PE film was highly hydrophobic with a contact angle of 135.6°. The water plasma treatment for 30 s significantly decreased the hydrophobicity of the VACNT/PE film, as reflected by the substantially reduced contact angle (86.4°, Figure 3B). Since it was hard to culture cells or even to modify DNA chains on the highly hydrophobic VACNT array, water plasma treatment could turn the pristine VACNT/PE film into a more amicable substrate for cell culture.

As shown in the Fourier transform infrared spectroscopy (FTIR) image (Figure 3C), the VACNT array did not exhibit any FTIR peak (curve a), indicating the lack of any function group. After water plasma treatment, a strong and broad FTIR peak appeared at around 3450 cm^{-1} for –OH (curve b). After adsorbing DNA onto VACNT array, the VACNT-DNA (curve d) exhibited several FTIR peaks overlapping with those of pure DNA (curve c),[15] indicating the successful modification of VACNT array with DNA.

2.3. Flexibility and Reproducibility of VACNT/PE Film

To examine the flexibility and stability of the VACNT/PE hybrid film, we investigated its bending and relaxing property. Figure 3D,E was photographs of the relaxing and bending conditions of VACNT/PE film, respectively. As shown in the short video (Video 1, Supporting Information), this film could almost retain its original shape after continuous bending/relaxing cycles. The excellent mechanical flexibility and stability of this free standing VACNT/PE film could benefit the emerging applications for in situ sensing of $O_2^{\bullet-}$ in the complex bioenvironment.

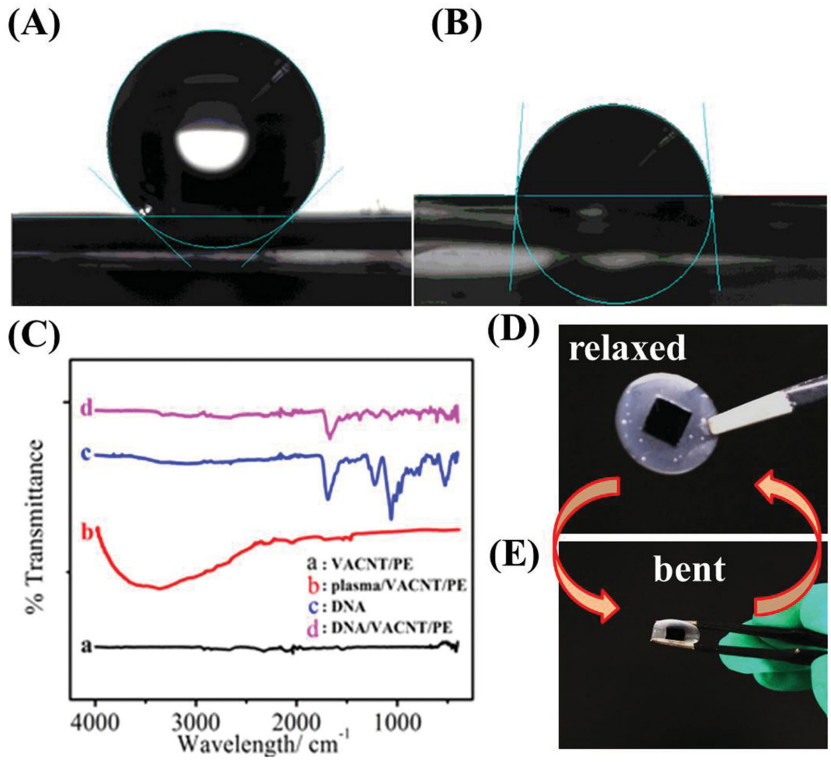

Figure 3. Contact angle test of VACNT/PE film A) before and B) after treatment with water plasma. C) FTIR image of a) VACNT array, b) water plasma treated VACNT array, c) pure DNA, and d) DNA/VACNT array. Photographs of the D) relaxing and E) bending conditions of VACNT/PE film.

2.4. Cell Adhesion on $Mn_3(PO_4)_2$/DNA/VACNT/PE Hybrid Film

Cell attachment and growth on the sensing matrix is critical for in situ detection of target biomolecules released from living cells. The surface property of the developed hybrid film for cell culture was investigated. After 24 h cell culture, 4′,6-diamidino-2-phenylindole, a highly specific and blue fluorescent dye, was applied to stain the cell nuclei in MDA-MB-231/VACNT/PE hybrid film and MDA-MB-231/$Mn_3(PO_4)_2$/DNA/VACNT/PE hybrid film, which were then visualized under a fluorescence microscope. As seen in **Figure 4**A, only a small number of cells could adhere on the pristine VACNT array. After water plasma treatment, the VACNT/PE film became more hydrophilic, and hence more suitable for subsequent modifications and cell attachment. This surface property change, together with DNA-induced formation of $Mn_3(PO_4)_2$ on VACNT/PE film, facilitated the growth of MDA-MB-231 cells on the resulting hybrid film. As shown in Figure 4B, many cells were observed on the 3D $Mn_3(PO_4)_2$/DNA/VACNT/PE hybrid film, indicating its excellent biocompatibility. Compared to the previous studies, this hybrid film promoted cell culture without further modification with extracellular matrix protein[8] or peptide graft.[16]

The anchorage-dependent cell adhesion was revealed by SEM. Figure 4C clearly displayed a cell attaching on the surface of VACNT/PE film, whereas few pseudopodia could be observed. In contrast, the cells cultured on $Mn_3(PO_4)_2$/DNA/VACNT/PE hybrid film exhibited many stretched pseudopodia (Figure 4D), indicating that the cell adhesion behavior was further enhanced by incorporating DNA and $Mn_3(PO_4)_2$.

2.5. Electrocatalytic Behaviors of $Mn_3(PO_4)_2$/DNA/VACNT/PE Hybrid Film

Cyclic voltammetry (CV) was applied to investigate the electrocatalytic property of the $Mn_3(PO_4)_2$/DNA/VACNT/PE sensing platform. As shown in Figure S2A (Supporting Information), electrocatalytic reaction between Mn(II) and Mn(III) species occurred on the surface of this film with an oxidative peak around 0.84 V and a reductive peak around 0.40 V in phosphate buffered saline (PBS) (0.01 M, pH 7.4). For $Mn_3(PO_4)_2$/VACNT/PE film, both oxidation and reduction peak currents reduced, which might be due to the lack of $Mn_3(PO_4)_2$ nanoparticles on VACNT array without the inducing effect of DNA (Figure S2B, Supporting Information). Figure S2C (Supporting Information) showed the CV performance of DNA/VACNT/PE, which only exhibited a polarization effect without any obvious redox peaks.

Compared to CV characterization, differential pulse voltammetry (DPV) technique has been proved to perform enhanced sensitivity by adding uncompensated resistance to the cell.[17] Considering the extremely short life time of $O_2^{\bullet-}$ produced by potassium superoxide (KO_2), DPV was applied to investigate $O_2^{\bullet-}$ oxidation on different modified films. As illustrated in **Figure 5**A, curve a, $Mn_3(PO_4)_2$/DNA/VACNT/PE hybrid film demonstrated an excellent electrocatalytic effect in response to 13×10^{-6} M $O_2^{\bullet-}$ in PBS (0.01 M, pH 7.4) with an oxidation peak at 0.55 V. The

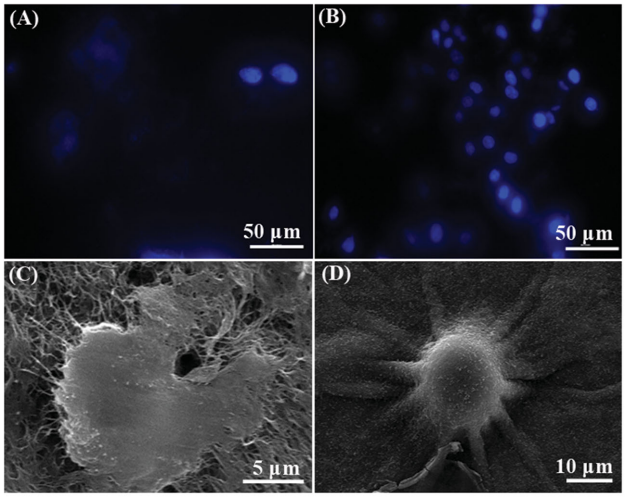

Figure 4. Fluorescence microscope images of MDA-MB-231 cells cultured on A) VACNT/PE and B) $Mn_3(PO_4)_2$/DNA/CNT/PE hybrid films. The SEM images of cells cultured on C) VACNT/PE and D) DNA/CNT/PE hybrid films.

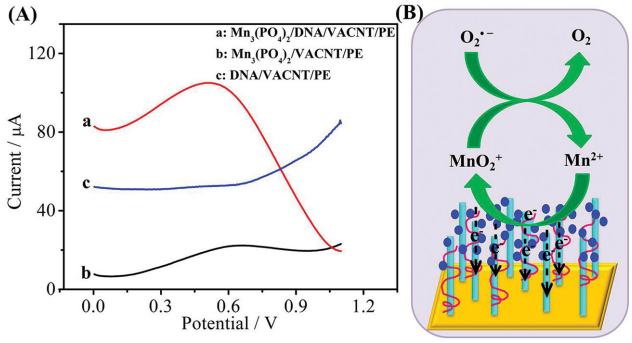

Figure 5. A) DPV measurements of different modified films in response to 13×10^{-6} M $O_2^{\bullet-}$ in PBS (0.01 M, pH 7.4): a) $Mn_3(PO_4)_2$/DNA/VACNT/PE hybrid film, b) $Mn_3(PO_4)_2$/VACNT/PE film, and c) DNA/VACNT/PE film. B) Scheme for oxidation mechanism of sensing hybrid film to $O_2^{\bullet-}$.

electrocatalytic mechanism of $Mn_3(PO_4)_2$ nanoparticles for $O_2^{\bullet-}$ was exhibited in Figure 5B. During this process, Mn^{2+} lost an electron to generate a short-lived transient MnO_2^+, then $O_2^{\bullet-}$ reduced MnO_2^+ to produce Mn^{2+} and O_2.[18]

Figure 5A, curve b, showed the response of $Mn_3(PO_4)_2$/VACNT/PE film in the presence of 13×10^{-6} M $O_2^{\bullet}$, which had a negligible current response compared to $Mn_3(PO_4)_2$/DNA/VACNT/PE film. Moreover, the DNA/VACNT/PE film did not show any obvious response to $O_2^{\bullet}$ (Figure 5A, curve c). Figure S2 (Supporting Information) demonstrated the DPV responses of different sensing films in pure PBS (curve a) and in response to 13×10^{-6} M $O_2^{\bullet-}$ (curve b), respectively. These results indicated that $Mn_3(PO_4)_2$ behaved as a biomimetic enzyme during $O_2^{\bullet-}$ catalysis. In addition, DNA was necessary for successful growth of $Mn_3(PO_4)_2$ on VACNT/PE film.

Selectivity and antiinterference ability of proposed hybrid film were studied by analyzing various interfering species, such as ascorbic acid (AA), K^+, Na^+, CO_3^{2-}, Cl^-, NO_3^-, uric acid (UA), nitric oxide (NO), hydrogen peroxide (H_2O_2), and hypochlorite (ClO^-). As seen in **Figure 6**A, the presence of AA, K^+, Na^+, CO_3^{2-}, NO_3^-, Cl^-, UA, NO up to 6.5 and 0.65×10^{-6} M of H_2O_2 as well as ClO^- did not cause any noticeable interference to the sensing hybrid film in response to 0.6×10^{-6} M $O_2^{\bullet-}$. The observed excellent selectivity was presumably due to the specific catalytic effect of the biomimetic superoxide dismutase ($Mn_3(PO_4)_2$) to $O_2^{\bullet-}$.

Chronoamperometry was employed to investigate the response of MDA-MB-231/$Mn_3(PO_4)_2$/DNA/VACNT/PE hybrid film to continuous addition of $O_2^{\bullet-}$ into PBS under an applied potential of 0.7 V. As shown in Figure 6B, a stepwise current response with increasing $O_2^{\bullet-}$ concentration was observed for the sensing hybrid film, reaching 95% of the steady-state current within 5 s. The short response time is an advantage for the real-time detection of $O_2^{\bullet-}$ released from living cells considering its short lifetime. The inset in Figure 6B showed a calibration curve of $O_2^{\bullet-}$ determination for the sensing hybrid film. The linear relationship was seen over two concentration ranges of $O_2^{\bullet-}$ from 65×10^{-9} to 4940×10^{-9} M and 5915×10^{-9} to $31\,590 \times 10^{-9}$ M with corresponding linear equations: I (μA) = 15.18 + 0.0012 C ($O_2^{\bullet-}$) (15.48 < I (μA) < 21.04) and I (μA) = 9.13 + 0.0026 C ($O_2^{\bullet-}$) (24.53 < I (μA) < 90.79), respectively

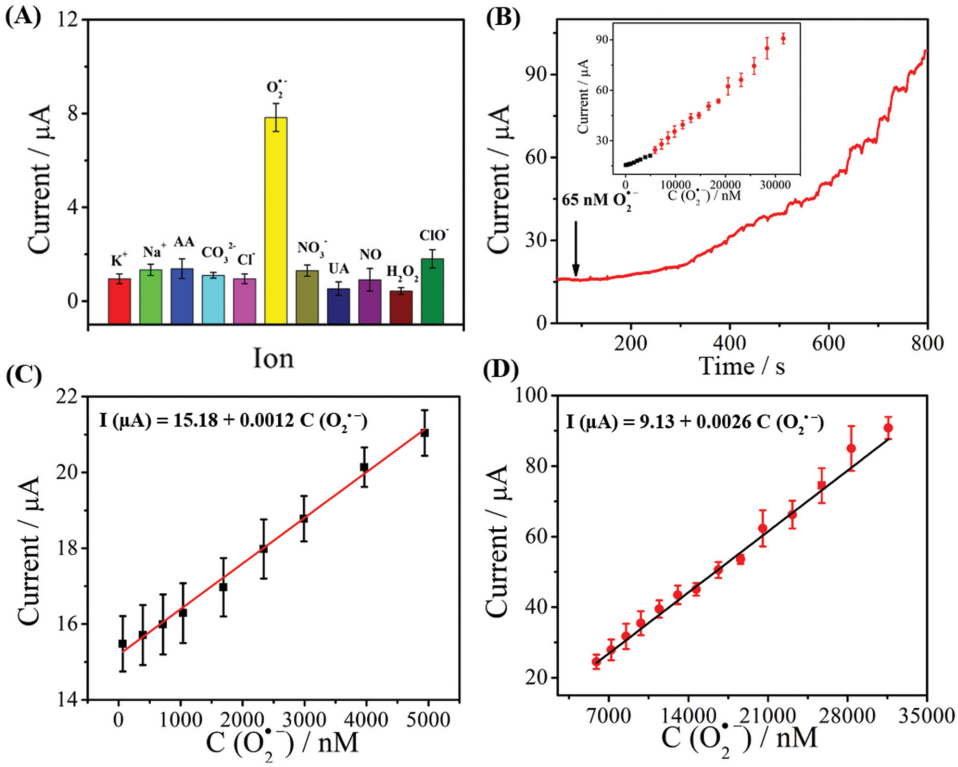

Figure 6. A) Selective performance of the hybrid film. B) Chronoamperometric response of the MDA-MB-231/$Mn_3(PO_4)_2$/DNA/VACNT/PE hybrid film in response to continuous addition of $O_2^{\bullet-}$ under an applied potential of 0.7 V. Inset of (B), (C), and (D) are linear plots for $O_2^{\bullet-}$.

(Figure 6C,D). The detection limit was estimated to be 30×10^{-9} M (S/N = 3), with sensitivity of 9.6 and 20.8 μA μM^{-1} cm^{-2} for these two linear ranges, respectively.

For comparison, chronoamperometry was employed to investigate the response of $Mn_3(PO_4)_2$/DNA/VACNT/PE hybrid film without cultured cells under the same condition (Figure S3A, Supporting Information). There was a linear relationship observed in two concentration ranges of $O_2^{\bullet-}$ from 65×10^{-9} to 5915×10^{-9} M and 7215×10^{-9} to $18\ 590 \times 10^{-9}$ M with corresponding linear equations: I (μA) = 7.89 + 0.0021 C ($O_2^{\bullet-}$) (8.44 < I (μA) < 20.61) and I (μA) = −23.78 + 0.0068 C ($O_2^{\bullet-}$) (27.91 < I (μA) < 99.06), respectively (Figure S3B–D, Supporting Information). The detection limit was estimated to be 28×10^{-9} M (S/N = 3) with sensitivity of 16.4 and 54.1 μA μM^{-1} cm^{-2} for these two linear ranges, respectively. This sensitivity was higher than that obtained for MDA-MB-231/$Mn_3(PO_4)_2$/DNA/VACNT/PE hybrid film. Apparently, the biological cells grown on $Mn_3(PO_4)_2$/DNA/VACNT/PE substrate could negatively affect $O_2^{\bullet-}$ diffusion from solution to access $Mn_3(PO_4)_2$ for oxidation, thus resulting in different detection range and sensitivity. It is worthy of a note that the measurements are only for calibration curves. When directly using the hybrid film to detect the generated ROS from the grown cells, no such an effect exists.

2.6. In Situ Detection of Superoxide Released from Living Cells

Quantitative in situ detection of released $O_2^{\bullet-}$ from cells grown on the proposed hybrid film was further performed. One of the deductive mechanisms implicated in zymosan (Zym, one of the drugs that can induce $O_2^{\bullet-}$ releasing from cell) activation on cells was illustrated in **Figure 7**A. Zym particles were

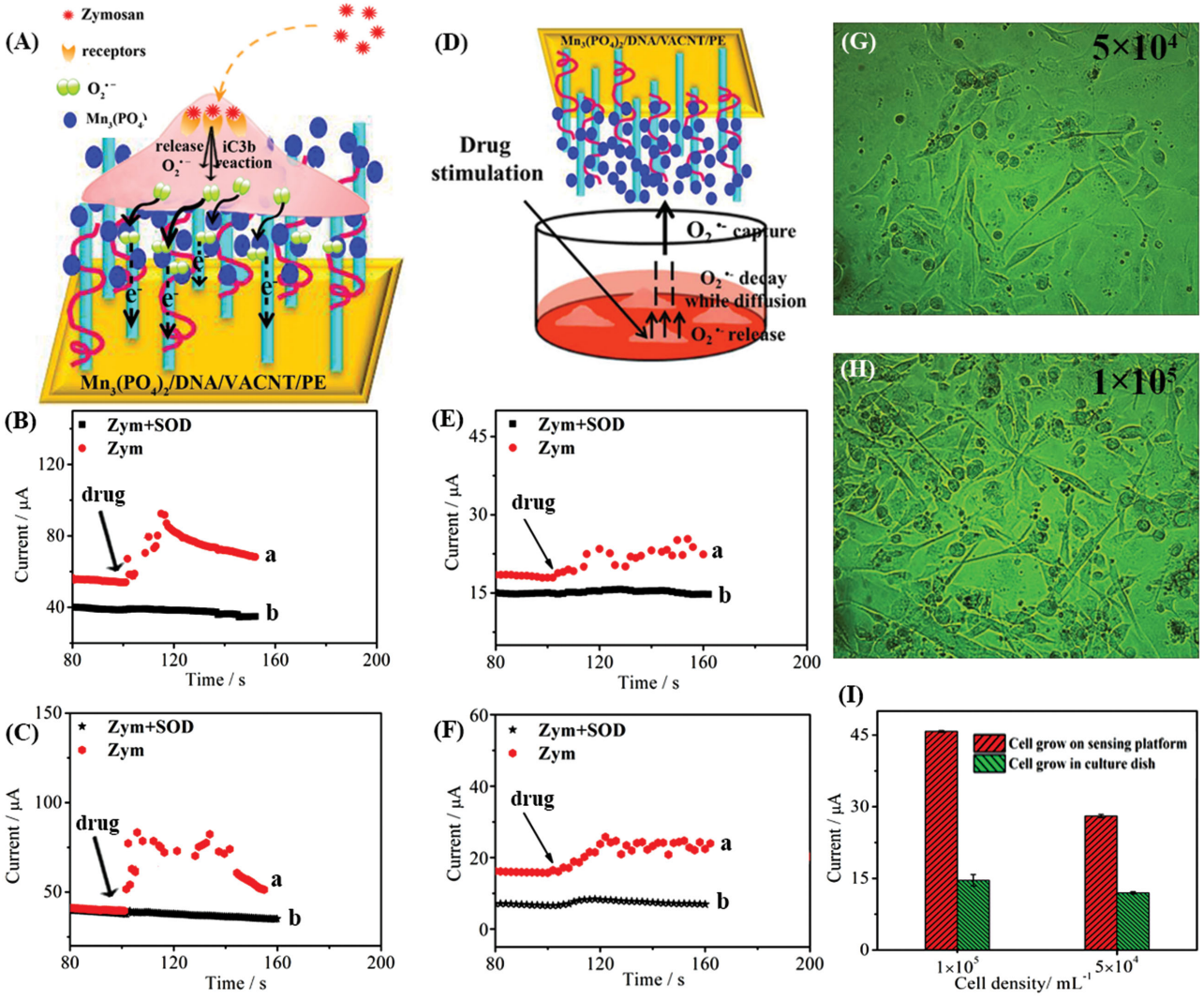

Figure 7. A) Scheme showing one path for Zym-triggered $O_2^{\bullet-}$ production from a human cell and timely capture of $O_2^{\bullet-}$ by the sensing platform. Chronoamperometry response of MDA-MB-231/$Mn_3(PO_4)_2$/DNA/VACNT/PE hybrid film to $O_2^{\bullet-}$ released by living MDA-MB-231 cells with cell density: B) 5×10^4 and C) 1×10^5 mL^{-1}. D) Scheme showing diffusion path of $O_2^{\bullet-}$ production from a human cell. Chronoamperometry response of $Mn_3(PO_4)_2$/DNA/VACNT/PE hybrid film to $O_2^{\bullet-}$ released by living MDA-MB-231 cells with cell density: E) 5×10^4 and F) 1×10^5 mL^{-1}. Microscopic images of MDA-MB-231 cells with cell density G) 5×10^4 and H) 1×10^5 mL^{-1} (magnification is 10×). I) The red or green bars correspond to current responses of cells grow on sensing platform or in a culture dish under drug stimulation.

Table 2. In situ detection of cell-released $O_2^{\bullet-}$ in different sensing hybrid films.

Sensing hybrid film	Cell density	Response time [s]	Concentration of $O_2^{\bullet-}$ released by cells [$\times 10^{-9}$ M]	$O_2^{\bullet-}$ number released by per cell
MDA-MB-231/$Mn_3(PO_4)_2$/DNA/VACNT/PE	5.0×10^4	5.25	13 437.58	9.71×10^{11}
	1.0×10^5	3.16	20 355.55	7.35×10^{11}
$Mn_3(PO_4)_2$/DNA/VACNT/PE	5.0×10^4	9.0	1966.99	5.92×10^{10}
	1.0×10^5	14.1	3243.69	4.88×10^{10}

first bound to receptors such as mannosyl and fucosyl. Then the composites were subjected to iC3b component activity and stimulated $O_2^{\bullet-}$ release.[19,20] Subsequently, the produced $O_2^{\bullet-}$ was directly captured by the sensing platform without solution diffusion path. To confirm the ROS generation of MDA-MB-231 cells treated with Zym, the ROS assay—dichloro-dihydro-fluorescein diacetate measurement[21] was performed. Results clearly showed that Zym-treated MDA-MB-231 cells produced ROS (Figure S4, Supporting Information). Figure 7B,C reproduced chronoamperometric responses of $Mn_3(PO_4)_2$/DNA/VACNT/PE hybrid film cultured with MDA-MB-231 cells for 24 h with cell density of 5.0×10^4 or 1.0×10^5 mL^{-1}, respectively, the current response were caused by ROS generation of MDA-MB-231 cells (Figure S4, Supporting Information). Upon addition of 1.0 mg mL^{-1} Zym (curve a), step currents were generated due to $O_2^{\bullet-}$ oxidation under cell density of 5.0×10^4 or 1.0×10^5 mL^{-1}, respectively. In contrast, the addition of 1.0 mg mL^{-1} Zym and 300 U mL^{-1} superoxide dismutase (SOD) (a selective scavenger of $O_2^{\bullet-}$) mixture did not cause any obvious current increase, indicating that the released $O_2^{\bullet-}$ molecules were consumed by SOD (curve b). From the drug-stimulated current response and the calibration equations for the sensing hybrid film, concentrations of the $O_2^{\bullet-}$ released from MDA-MB-231 cells under cell densities of 5.0×10^4 and 1.0×10^5 mL^{-1} were calculated as 13 437.58 $\times 10^{-9}$ and 20 355.55 $\times 10^{-9}$ M, respectively. The $O_2^{\bullet-}$ concentration released by MDA-MB-231 cells under density of 1.0×10^5 mL^{-1} were about 1.5 times than that under density of 5.0×10^4 mL^{-1}. Figure 7G,H was the microscopic images of MDA-MB-231 cells under different cell densities. Furthermore, the average number of extracellular $O_2^{\bullet-}$ molecules released per cell (N_0) can be calculated according to Avogadro equation ($n = N_0/N_A$, $N_A = 6.02 \times 10^{23}$ mole^{-1}). Given the total amount of released $O_2^{\bullet-}$, cell density, and the volume of electrolyte (6 mL), N_0 was calculated as 9.71×10^{11} and 7.35×10^{11} for cell densities of 5.0×10^4 and 1.0×10^5 mL^{-1}, respectively (**Table 2**).

Figure 7D is a schematic process of cell-released $O_2^{\bullet-}$ detection with $Mn_3(PO_4)_2$/DNA/VACNT/PE hybrid film while cells are cultured in a petri dish. In contrast to MDA-MB-231 cells directly grown on the sensing hybrid film, $O_2^{\bullet-}$ released from living cells at the bottom of petri dish under drug stimulation need to diffuse through the medium to reach the surface of sensing platform. Because $O_2^{\bullet-}$ molecules are by nature very active, most of them will decay during this process. Figure 7E,F exhibited the responses of $Mn_3(PO_4)_2$/DNA/VACNT/PE to MDA-MB-231 cells under drug effect with cell density of 5.0×10^4 or 1.0×10^5 mL^{-1}, respectively. However, the obtained current step intensities were much weaker, indicating less $O_2^{\bullet-}$ were captured upon the same drug stimulation (Figure 7I). The total concentrations of released $O_2^{\bullet-}$ by all cells and the number of $O_2^{\bullet-}$ molecules per cell are calculated and summarized in Table 2. Under cell densities of 5.0×10^4 or 1.0×10^5 mL^{-1}, the measured total concentrations of $O_2^{\bullet-}$ released by all cells directly grown on the sensing hybrid film was about 6.8 and 6.3 times of those by cells cultured in a petri dish, respectively. As for the number of $O_2^{\bullet-}$ molecules released per cell, the former one produced more reliable results as 9.71×10^{11} and 7.35×10^{11}, which were 16.4 and 15.1 times of those obtained by the latter one. These results showed that $O_2^{\bullet-}$ molecules secreted from living MDA-MB-231 cells could be immediately captured by the MDA-MB-231/$Mn_3(PO_4)_2$/DNA/VACNT/PE smart film without a diffusion process or with short diffusion length compared to cells growing in culture dish conventionally, which could be further confirmed by much shorter response times of the former one (Figure S5, Supporting Information), providing enhanced in situ detection with much higher sensitivity and reliability.

Apparently, the superior performance of detection of $O_2^{\bullet-}$ in situ in this work should attributed to the smart free-standing hybrid film made from directly grow living cells on the DNA/$Mn_3(PO_4)_2$-immobilized and VACNT array nanostructure, of which the DNA/$Mn_3(PO_4)_2$ and VACNT provides high electroactivity and excellent electron transport ability, respectively, while the directly grown cell on the nanostructure offers short diffusion distance to the reaction sites for high sensitivity, excellent specificity, and wide dynamic range.

3. Conclusion

Using water-plasma treatment followed by DNA-induced deposition of $Mn_3(PO_4)_2$ onto vertically aligned CNT arrays, we have developed a unique approach to fabricate a $Mn_3(PO_4)_2$/DNA/VACNT/PE hybrid film for direct cell culture and detection of cell-released $O_2^{\bullet-}$ in situ with good catalytic activity and selectivity. Compared to the traditional detection of ROS molecules released by cells that are cultured in a petri dish, this proposed sensing platform delivers superior performance because of the constructed smart nanostructured hybrid film. Therefore, this work holds great promise for further development of many living cell-based biological assays, such as cellular functions, drug discovery, pathology, and toxicology.

4. Experimental Section

Reagents and Chemicals: DNA (low molecular weight, from salmon sperm), manganese sulfate ($MnSO_4$) and potassium phosphate tribasic

(K_3PO_4), potassium superoxide (KO_2), SOD (from bovine erythrocytes), Zymosan A (Zym, from Saccharomyces cerevisiae), PE, 0.01 M pH 7.4 PBS were obtained from Sigma-Aldrich. Sterile Advanced MEM medium, penicillin, and fetal bovine serum are obtained from Life Technologies. The $O_2^{\bullet-}$ solutions were prepared by the addition of KO_2 solid powder to PBS (N_2 saturated). The concentration of $O_2^{\bullet-}$ was determined by recording the reduction of ferri cytochrome c spectrophotometrically and using the extinction coefficient (21.1 mM^{-1} cm^{-1}) of ferrocytochrome c at 550 nm.[22] All other chemicals were purchased from Sigma and used as obtained. Deionized water was used throughout the experiments.

VACNT arrays were synthesized by low pressure chemical vapor deposition of C_2H_2 on SiO_2 (400 nm)/Si wafers.[23] A 10 nm thick Al layer was precoated on the wafers before the deposition of 3 nm Fe film. The catalyst-coated substrate was first inserted into a quartz tube furnace and heated up to 650 °C in air, followed by pumping the furnace chamber to a pressure below 30 mTorr. The VACNT arrays were then grown by flowing a gas mixture of 50% Ar, 25% H_2, and 25% C_2H_2 at 750 °C under 100 Torr through the quartz tube furnace for 10–20 min. The nanotube length of the VACNT arrays were measured with SEM, and VACNT arrays with a length of about 80 μm were selected in this experiment, which were sputter coated with a 400 nm thick gold layer to enhance the conductivity.

Apparatus: The electrochemical measurements were performed on a CHI 760e electrochemical work station (Shanghai, China). The conventional three-electrode system includes a modified hybrid film as working electrode, an Ag/AgCl reference electrode, and a platinum wire as counter electrode. Scanning electron images were recorded on a scanning electron microscope (Tescan SEM). The contact angle measurements were performed on OCA 15EC, Dataphysics. Water plasma treatment was done with Custom Built RF plasma Reactor. Fourier transform infrared spectroscopy was carried out with PerkinElmer FT-IR C93160. XPS measurements were performed on a VG Microtech ESCA 2000 using a monochromic Al X-ray source (76.0 W, 93.9 eV). Fluorescence images were taken with Olympus IX71 with a fluorescent light from Olympus TH4-100. Sputter coating was done with Explore 14.

Preparation of the Hybrid Film: In a typical experiment, an appropriate polymer (PE) thin film with a thickness of around 200 μm was placed on the top surface of a silicon substrate, and the VACNT array was then transferred upside down onto the top of polymer film (gold layer facing to the polymer). Upon heating at 200 °C for 2 min, the polyethylene was infiltrated into VACNT array to form free standing VACNT/PE film. After cooled down to room temperature, VACNT/PE film was peeled off from the silicon substrate. Subsequently, water plasma was applied to improve the hydrophilicity of VACNT/PE film.

DNA (200 mg) powder was added to deionized water (20 mL) under stirring. Upon heating to 95 °C, the DNA solution was stirred for another 15 min and then quickly cooled down in ice water to produce single-stranded DNA chains, which were stored at 4 °C when not in use. Then water plasma treated VACNT/PE film was dipped into single-stranded DNA solution, and the incubation was carried out by mild shaking the mixture for 3 h (shown in Scheme 1).

Through the specific electrostatic interaction between Mn^{2+} and negatively charged DNA, Mn^{2+} were assembled onto the DNA/VACNT/PE film for in situ growth of $Mn_3(PO_4)_2$ by immersing DNA/VACNT/PE film into 0.1 M $MnSO_4$ and 0.1 M K_3PO_4 solution consecutively. Finally, the free standing $Mn_3(PO_4)_2$/DNA/VACNT/PE film was applied to culture MDA-MB-231 cells to fabricate a hybrid film for detecting $O_2^{\bullet-}$ released by living cells through drug stimulation. In order to conduct the electrochemical experiment, titanium wire was assembled onto the testing film with silver paste to connect with electrochemical analysis station. $Mn_3(PO_4)_2$ directly modified VACNT/PE film was also fabricated with the same method in the absence of DNA.

Cell Culture on $Mn_3(PO_4)_2$/DNA/VACNT/PE Film: MDA-MB-231 cells were cultured in a humidified incubator (95% air with 5% CO_2) at 37 °C in culture medium, which was prepared by mixing sterile Advanced MEM medium, 1% penicillin and 10% fetal bovine serum. MDA-MB-231 cells were cultured in a petri dish (Ø = 60 mm) with the as-prepared culture medium and controlled under different cell densities, such as 5.0×10^4 and 1.0×10^5 mL^{-1}.

To investigate cell adhesion behavior on the VACNT/PE film and $Mn_3(PO_4)_2$/DNA/VACNT/PE film, sterilization was done by treating them with 70% alcohol and UV light prior to cell culture. After that, the sterilized VACNT/PE film and $Mn_3(PO_4)_2$/DNA/VACNT/PE film were submerged into Advance minimum essential medium (MEM) to seed MDA-MB-231 cells for further experiments.

Supporting Information

Supporting Information is available from the Wiley Online Library or from the author.

Acknowledgements

The authors would like to gratefully acknowledge the financial support from the 973 program of China (Grant No. 2013CB127804), Chongqing Key Laboratory for Advanced Materials and Technologies of Clean Energies, Start-up grant under SWU111071 from Southwest University, Chongqing Engineering Research Center for Rapid Diagnosis of Dread Disease and Chongqing development and reform commission and China Scholarship Council.

Received: June 9, 2015
Revised: July 30, 2015
Published online: August 25, 2015

[1] a) H. A. Kontos, E. P. Wei, *J. Neurosurg.* **1986**, *64*, 803; b) H. Ji, H. Li, P. Martásek, L. J. Roman, T. L. Poulos, R. B. Silverman, *J. Med. Chem.* **2009**, *52*, 779.
[2] a) J. L. Zweier, M. A. H. Talukder, *Cardiovasc. Res.* **2006**, *70*, 181; b) M. Ganesana, J. S. Erlichman, S. Andreescu, *Free Radicals Biol. Med.* **2012**, *53*, 2240.
[3] B. A. Freeman, J. D. Crapo, *Lab. Invest.* **1982**, *47*, 412.
[4] W. A. Pryor, S. S. Godber, *Free Radicals Biol. Med.* **1991**, *10*, 177.
[5] a) K. Barnese, E. B. Gralla, J. S. Valentine, D. E. Cabelli, *Proc. Natl. Acad. Sci. USA* **2012**, *109*, 6892; b) R. L. McNaughton, A. R. Reddi, M. H. S. Clement, A. Sharma, K. Barnese, L. Rosenfeld, E. B. Gralla, J. S. Valentine, V. C. Culotta, B. M. Hoffman, *Proc. Natl. Acad. Sci. USA* **2010**, *107*, 15335.
[6] X. Ma, W. Hu, C. Guo, L. Yu, L. Gao, J. Xie, C. M. Li, *Adv. Funct. Mater.* **2014**, *24*, 5897.
[7] R. M. Wightman, *Science* **2006**, *311*, 1570.
[8] C. X. Guo, X. T. Zheng, Z. S. Lu, X. W. Lou, C. M. Li, *Adv. Mater.* **2010**, *22*, 5164.
[9] M. Ebara, M. Yamato, T. Aoyagi, A. Kikuchi, K. Sakai, T. Okano, *Adv. Mater.* **2008**, *20*, 3034.
[10] K. Gong, F. Du, Z. Xia, M. Durstock, L. Dai, *Science* **2009**, *323*, 760.
[11] T. Chen, H. Peng, M. Durstock, L. Dai, *Sci. Rep.* **2014**, *4*, 3612.
[12] Z. Tao, P. Wang, L. Wang, L. Xiao, F. Zhang, J. Na, *J. Mater. Chem. B* **2014**, *2*, 471.
[13] a) M. Zheng, A. Jagota, M. S. Strano, A. P. Santos, P. Barone, S. G. Chou, B. A. Diner, M. S. Dresselhaus, R. S. Mclean, G. B. Onoa, G. G. Samsonidze, E. D. Semke, M. Usrey, D. J. Walls, *Science* **2003**, *302*, 1545; b) X. Tu, S. Manohar, A. Jagota, M. Zheng, *Nature* **2009**, *460*, 250.
[14] M. R. Vilar, A. M. Botelho do Rego, A. M. Ferraria, Y. Jugnet, C. Noguès, D. Peled, R. Naaman, *J. Phys. Chem. B* **2008**, *112*, 6957.

[15] H. D. A. Mohamed, S. M. D. Watson, B. R. Horrocks, A. Houlton, *Nanoscale* **2012**, *4*, 5936.
[16] a) C. X. Guo, S. R. Ng, S. Y. Khoo, X. Zheng, P. Chen, C. M. Li, *ACS Nano* **2012**, *6*, 6944; b) H. Asakawa, K. Mochitate, T. Haruyama, *Anal. Chem.* **2008**, *80*, 1505.
[17] A. P. Brown, F. C. Anson, *Anal. Chem.* **1977**, *49*, 1589.
[18] J. Zhou, Y. Luo, A. Zhu, Y. Liu, Z. Zhu, Y. Tian, *Analyst* **2011**, *136*, 1594.
[19] R. A. B. Ezekowitz, R. B. Sim, M. Hill, S. Gordon, *J. Exp. Med.* **1984**, *159*, 244.
[20] Q. Y. Lin, L. J. Jin, Z. H. Cao, Y. N. Lu, H. Y. Xue, Y. P. Xu, *Phytother. Res.* **2008**, *22*, 740.
[21] A. Aranda, L. Sequedo, L. Tolosa, G. Quintas, E. Burello, J. V. Castell, L. Gombau, *Toxicol. In Vitro* **2013**, *27*, 954.
[22] J. M. McCord, I. Fridovich, *J. Biol. Chem.* **1969**, *244*, 6049.
[23] L. Qu, L. Dai, M. Stone, Z. Xia, Z. L. Wang, *Science* **2008**, *322*, 238.